Identification of Topotactic Surface-Confined Ullmann-Polymerization

Dominik Dettmann, Gianluca Galeotti, Oliver Maclean, Massimo Tomellini, Marco Di Giovannantonio, Josh Lipton-Duffin, Alberto Verdini, Luca Floreano, Yannick Fagot-Revurat, Dmitrii F. Perepichka, et al.

Identification of Topotactic Surface-Confined Ullmann-Polymerization

Dominik Dettmann, Gianluca Galeotti, Oliver MacLean, Massimo Tomellini, Marco Di Giovannantonio, Josh Lipton-Duffin, Alberto Verdini, Luca Floreano, Yannick Fagot-Revurat, Dmitrii F. Perepichka, Federico Rosei,* and Giorgio Contini**

On-surface Ullmann coupling is an established method for the synthesis of 1D and 2D organic structures. A key limitation to obtaining ordered polymers is the uncertainty in the final structure for coupling via random diffusion of reactants over the substrate, which leads to polymorphism and defects. Here, a topotactic polymerization on Cu(110) in a series of differently-halogenated para-phenylenes is identified, where the self-assembled organometallic (OM) reactants of diiodobenzene couple directly into a single, deterministic product, whereas the other precursors follow a diffusion driven reaction. The topotactic mechanism is the result of the structure of the iodine on Cu(110), which controls the orientation of the OM reactants and intermediates to be the same as the final polymer chains. Temperature-programmed X-ray photoelectron spectroscopy and kinetic modeling reflect the differences in the polymerization regimes, and the effects of the OM chain alignments and halogens are disentangled by Nudged Elastic Band calculations. It is found that the repulsion or attraction between chains and halogens drive the polymerization to be either diffusive or topotactic. These results provide detailed insights into on-surface reaction mechanisms and prove the possibility of harnessing topotactic reactions in surface-confined Ullmann polymerization.

1. Introduction

On-surface synthesis is a promising approach to obtain low-dimensional organic materials that exhibit appealing combinations of properties, including a tunable bandgap or high charge-carrier mobility, as well as intriguing features, such as Dirac cones,[1] carbon magnetism,[2] and topological states.[3] These materials can be synthesized by various surface mediated reactions, such as Schiff-base condensation,[4] Sonogashira coupling,[5] alkyne coupling,[6] photocycloaddition,[7] and Ullmann coupling.[8] Among these, the most-widely explored so far is the on-surface Ullmann-type reaction,[9] which has been used (in combination with cyclodehydrogenation) to create a range of graphene nanoribbons[10] and porous graphene.[1,11] The general pathway of on-surface Ullmann polymerization

D. Dettmann, G. Galeotti,[+] O. MacLean, F. Rosei
Centre Énergie
Matériaux et Télécommunications
Institut National de la Recherche Scientifique Department
1650 Boulevard Lionel-Boulet, J3X1S2, Varennes, Québec, Canada
E-mail: oliver.maclean@inrs.ca; rosei@inrs.ca

G. Galeotti, M. Di Giovannantonio, G. Contini
Istituto di Struttura della Materia
Consiglio Nazionale delle Ricerche
Via Fosso del Cavaliere 100, Roma 00133, Italy
E-mail: giorgio.contini@ism.cnr.it

O. MacLean
Key Laboratory of Functional Materials Physics and Chemistry
of the Ministry of Education
Jilin Normal University
Changchun 130103, P. R. China

M. Tomellini
Department of Chemistry
University Tor Vergata
Via della Ricerca Scientifica 1, Roma 00133, Italy

J. Lipton-Duffin
School of Chemistry and Physics
Queensland University of Technology
2 George Street, Brisbane 4001 QLD, Australia

A. Verdini, L. Floreano
Istituto Officina dei Materiali
Consiglio Nazionale delle Ricerche
S.S. 14, km 163.5, Trieste I-34149, Italy

Y. Fagot-Revurat
Institut Jean Lamour Campus ARTEM UMR 7198
CNRS-Université de Lorraine
2 allée André Guinier, BP 50840, Nancy 54011, France

D. F. Perepichka
Department of Chemistry
McGill University
801 Sherbrooke Street West, Montreal, QC H3A 0B8, Canada

G. Contini
Department of Physics
University Tor Vergata
Via della Ricerca Scientifica 1, Roma 00133, Italy

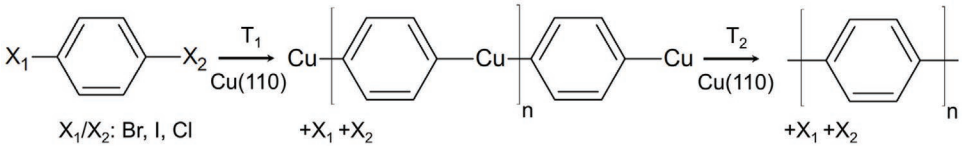

Scheme 1. On-surface Ullmann reaction of 1,4-dihalobenzene on Cu(110).

has been shown to involve two steps: 1) homolytic cleavage of the C—X bond (X: Br, Cl, I), with the carbon radical stabilized by the metal substrate (either as a stable organometallic (OM) phase or a metastable intermediate) and 2) thermally-activated carbon-carbon (C—C) coupling of dehalogenated molecules to form a covalent polymer.[8a,9a,12] **Scheme 1** shows this pathway for 1,4-dihalobenzene molecules on Cu(110), which form intermediate OM chains with Cu atoms between every phenylene group.

However, ordered polymer domains to date have been limited in spatial extension, hindering their use in applications.[13] Achieving polymers with improved order and domain size calls for an in-depth understanding of the on-surface polymerization reaction mechanisms.[9c,14] The rate of diffusion relative to coupling of the organic species influences the order of the polymer product, with coupling-limited processes yielding more ordered structures than diffusion-limited reactions, as shown in a comparative study of different surfaces combined with Monte Carlo simulations.[9a] However, coupling driven by random molecular diffusion introduces uncertainty into the polymerization process that is reflected in polymorphism or defects.[1,9c,15]

Topotactic reactions offer a means to suppress these undesirable effects. In this mechanistic regime, diffusion is restricted and the reactant molecules are organized to directly convert into the product,[16] as reported for photopolymerization of diacetylene molecules[17] and suggested for Ullmann polymerization of dibromodiphenylacetylene.[18] Although topotactic reaction offers greater predictability that could benefit the design and synthesis of long-range-ordered polymers, the driving forces that determine topotactic or diffusive pathways have not been investigated so far. The broad range of choice in molecular backbone, functional group and metal surface and their complex interplay introduces a high degree of unpredictability into on-surface reactions. To identify general rules for on-surface Ullmann-like reactions, it is necessary to carry out systematic studies by varying key parameters.[19]

In previous work, we showed that the conversion of 1,4-dibromobenzene (dBB) from OM chains to poly(*para*-phenylene) (PPP) chains on Cu(110) occurs in the diffusive regime.[20] In subsequent work, we investigated a series of additional precursors and their reaction to PPP by Ullmann polymerization on Cu(110), namely 1,4-dichlorobenzene (dCB), 1,4-diiodobenzene (dIB), 1-bromo-4-iodobenzene (BIB), and 1-bromo-4-chlorobenzene (BCB). This study revealed that the halogen controls the alignments of the OM chains: chlorine- and bromine-containing precursors yield OM chains following the [1 –1 ±1] surface direction, while OM chains resulting from dIB align along the [1 –1 ±2] direction. This is likely caused by the adsorption of bromine and chlorine at short-bridge positions, whereas iodine prefers hollow positions. After polymerization, the PPP chains follow either the [1 –1 ±2] or [1 –1 0] surface direction, implying a change in orientation compared with the initial chains for dBB, dCB, BIB, and BCB. In addition, we identified differences in the onset temperatures for polymerization; however, the mechanisms that underpin these differences and whether diffusion driven kinetics is the general mechanism for on-surface Ullmann coupling remained unknown.[21]

Here, we identify two distinct mechanistic regimes of polymerization on Cu(110), either diffusive or topotactic, by following the polymerization progress in real-time using temperature-programmed X-ray photoelectron spectroscopy (TP-XPS). In addition, we employ scanning tunneling microscopy (STM) and density functional theory (DFT) modeling using the Nudged Elastic Band (NEB) method to reveal key differences between the mechanistic pictures of these systems and identify the elementary steps that cause the change in kinetics. We demonstrate that the Ullmann polymerization of dIB follows a topotactic reaction pathway, in which the orientation of the OM chains determines the direction of the PPP chains and the reaction occurs through a strict 1D coupling process along the [1 –1 ±2] surface direction. In contrast, dCB, BCB, and BIB follow the coupling-limited nucleation and growth mechanism previously identified for dBB, where the OM self-assembly along the [1 –1 ±1] surface direction breaks and the PPP chains are formed along [1 –1 ±2].[21] The change of reaction mechanism upon varying the leaving group is a textbook example of mechanistic organic chemistry (e.g., transition from S_N2 to S_N1 mechanism in nucleophilic substitution of alkylhalides). However, the effect of the halogen leaving group on the kinetics of on-surface Ullmann coupling is unexpected considering that it is fully detached from the monomer molecules *before* the rate limiting (C—C coupling) step. The NEB calculations confirm that the halogen atoms do not only determine the orientation of the organometallic assembly but also affect the activation energies. Our findings underscore the advantages of TP-XPS in conjunction with kinetic models and NEB pathway analysis to obtain a complete mechanistic picture of surface reactions that accounts for the role of each reactant and side product.

2. Results and Discussion

To gain insights into the polymerization process of on-surface Ullmann coupling, we performed a kinetic analysis of TP-XPS maps revealing the chemical evolution from the OM to the PPP phase of dBB, dCB, dIB, BCB, and BIB on Cu(110), which were captured by acquiring XPS spectra of the C 1s core level, while progressively increasing the surface temperature (**Figure 1**a; and Figure S1, Supporting Information).[20,21] All TP-XPS maps were recorded at monolayer coverage to compare the precursors without coverage-dependent effects.[22] Experimental details on the coverage, adsorption stoichiometry and extraction of kinetic

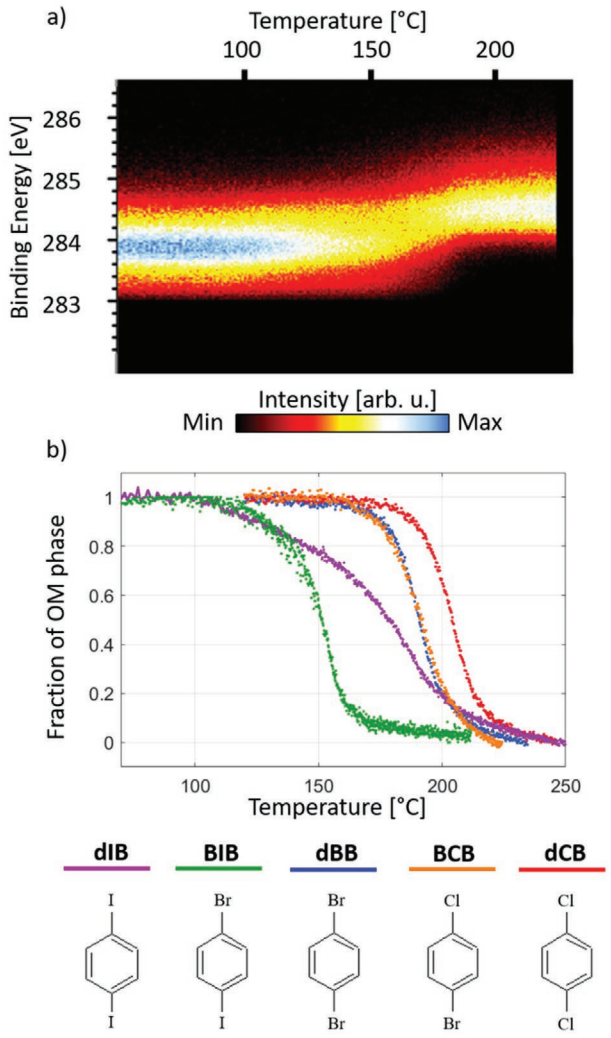

Figure 1. Extraction of kinetic information from TP-XPS maps. a) TP-XPS map of the temperature evolution of the C 1s core level signal for dIB. The monotonic shift toward higher binding energies indicates the transition from OM to polymer phase. b) Kinetic curves obtained from deconvolution of TP-XPS maps of Figure S1 (Supporting Information) following the procedure described in Section 1 (Supporting Information). dBB, dCB, BCB, and BIB exhibit a sharp transition within a limited temperature interval. dIB (magenta curve) shows a gradual conversion of OM into the polymer phase, in a much larger temperature range. Bottom: molecular structures of the investigated molecules.

data can be found in Section 1 (Supporting Information). While dBB, dCB, BCB, and BIB undergo a sharp reaction, limited to an interval of about 50 °C, dIB's transition is more gradual and occurs over a broad temperature range of about 110 °C (Figure 1b). An additional difference is the onset temperature of the reaction, as dBB, dCB, and BCB's phase transitions start in a temperature region of about 166–185 °C, while iodine-containing precursors start the reaction at 110–115 °C.

It has been shown that the Ullmann reaction in the case of dBB on Cu(110) proceeds as a nucleation and growth (NG) mechanism,[20] in which monomers randomly diffuse on the surface and couple to form dimers (nucleation) or attach to existing oligomers to produce longer chains (growth).

The nucleation process was modeled using two elementary steps. First, an organometallic phenylene moiety goes into a transient state. From this state, it can either couple with another activated phenylene to form a dimer or back diffuse to restore the original OM state. Thus, the transient state introduces a reversible process similar to the classic theory of nucleation and growth, in which a nucleus is unstable until it reaches a certain critical size. The growth of longer oligomers proceeds similarly and also includes the transition of an organometallic phenylene into the transient state and its subsequent coupling to an existing oligomer chain. The rates into and out of the transient state control the coupling process and its classification from coupling-limited (where back-diffusion is favored) to diffusion-limited (where coupling is favored) polymerization.[9a,b,20] E_n and E_g are the respective activation energies for nucleation and growth (Section 2, Supporting Information). In the case of dBB on Cu(110), the experimental kinetics of the polymerization process is best described by preferential back-diffusion.[20]

We investigated the kinetics of the polymerization process of all five precursors by considering the coupling-limited NG model, which previously gave the best agreement for dBB on Cu(110), represented by the following set of Equation (1)

$$\begin{cases} \dfrac{d\eta}{dT} = k_n\, x_1^2 \\ \dfrac{dx_1}{dT} = -2k_n x_1^2 - k_g \eta x_1 \end{cases} \quad (1)$$

where x_1 is the density of phenylenes normalized to their initial density in the OM phase and η is the density of nuclei normalized to the initial density of phenylenes. k_n and k_g are effective rate constants for the nucleation and growth process. A complete derivation of our kinetic model can be found in Section 2 (Supporting Information), while the explanation and discussion of the fitting procedure are described in Section 3 (Supporting Information). The NG-kinetic approach yields good fits for dBB, dCB, BIB, and BCB (**Figure 2**) and the activation energies for nucleation and growth are summarized in **Table 1**. dBB, dCB, and BCB exhibit comparable nucleation energies E_n around 1.3 eV, whereas BIB has a lower nucleation energy of 1.15 eV. The systematic overestimation toward the final OM conversion for dBB, dCB, BCB, and BIB likely occurs once free monomers have been exhausted and further growth of the PPP chains occurs by coupling of oligomers, which is not accounted for in the rate equations.

For dIB, however, the coupling-limited NG polymerization mechanism gives a low-quality fit (Figure 2c), suggesting a different reaction pathway. To explore alternative mechanisms for the organometallic conversion of dIB, we investigated zero, first, second and *m*th-order kinetic equations with a single coupling step. Zero-order kinetics describe chemical changes in which the reaction rate does not depend on the number of reactants and model topotactic reactions, whereas first, second and *m*th order reaction kinetics account for diffusion.[20] However, using a single reaction order term it was not possible to reproduce the experimental data (Figure S5, Supporting Information). This prompted us to take into account other factors to improve our microscopic description of the polymerization process for dIB.

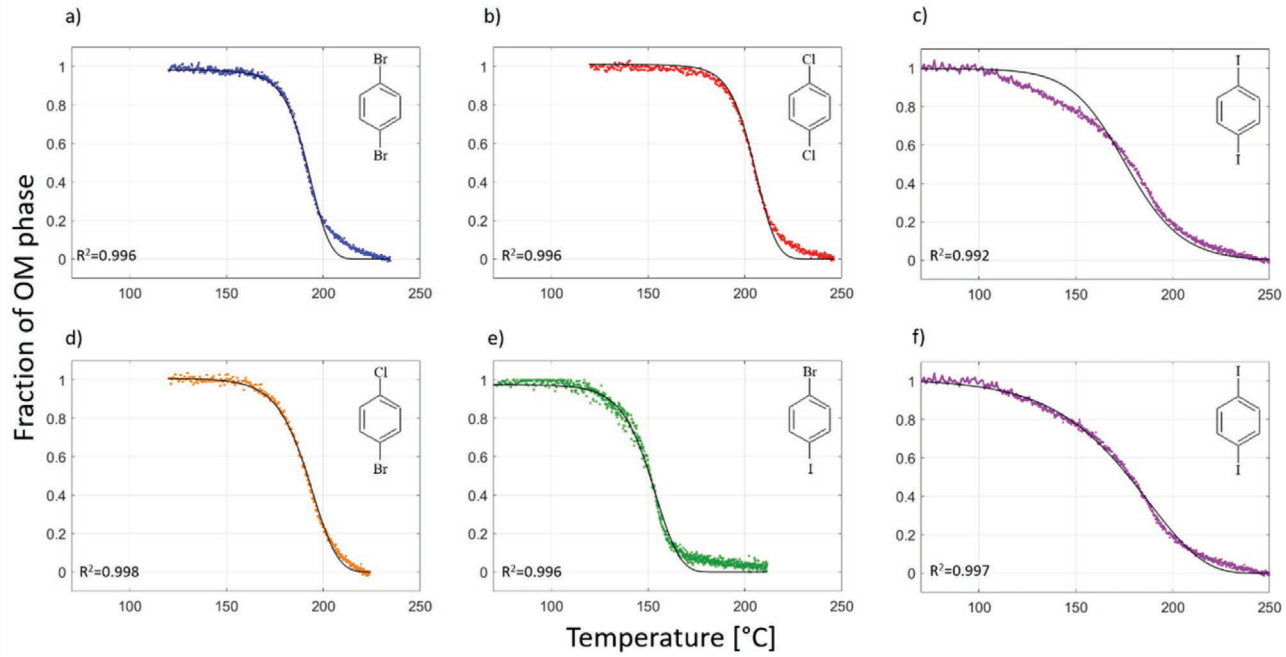

Figure 2. Kinetic analysis of dBB, dCB, BCB, BIB, and dIB: a–e): Fits obtained by the coupling-limited nucleation and growth mechanism (black lines) are in good agreement with the experimental curves of dBB, dCB, BCB, and BIB (colored dots). The experimental kinetic curve of dIB cannot be reproduced by this coupling-limited nucleation and growth model. f) Fit obtained by 1D-KJMA (black line) matches the kinetic curve of dIB (colored dots).

To this end, we studied the evolution of polymer chains arising from dIB molecules on Cu(110) through step-wise annealing of the surface at 100, 200, and 250 °C (**Figure 3**a–d). The blue box in Figure 3a shows a segment of an OM chain that consists of repeating units of Cu atoms (dots) and phenylenes (in between dots, detailed structure in the inset of Figure 3a) and follows the [1 −1 ±2] surface direction. The linear features between two OM chains are adsorbed iodine atoms. Annealing at 200 °C induces conversion of the OM phenylenes into small oligomers, connected by Cu atoms (as shown by the white box in Figure 3b), and polymer chains (as indicated by the black box). Figure 3c shows the polymer chains when conversion of the phenylene monomers is nearly complete (as shown by the yellow boxes). After annealing at 250 °C, longer polymer chains have formed, as indicated by the black box. This series of STM images shows that the intermediate oligomers and polymers align along the same [1 −1 ±2] surface direction as the OM precursor chains, which is consistent with topotactic conversion.

In the early stages of the reaction, only small oligomers are created (mostly from 2 to 5 phenylenes Figure 3b), and their merging into longer PPP chains (Figure 3d) requires increased temperatures and/or longer reaction times. This suggests that the reaction mechanism should incorporate two steps: first, the phenylenes form oligomers in a "zip" process, which requires limited molecular movement because the phenylenes are consecutive and aligned correctly to react; second, OM conversion is completed by diffusion along [1 −1 ±2] and coupling of the adjacent oligomers to form long PPP chains. This type of mechanism can be described using a 1D Kolmogorov–Johnson–Mehl–Avrami (1D-KJMA) model that considers the reaction ruled by irreversible growth and includes fusion of adjacent nuclei (in our case, these nuclei represent oligomers).[23] Figure 3 suggests the presence of two overlapping regimes, in which reaction is at first driven by the conversion of monomers and subsequently by the fusion of oligomers. The inflection point of the kinetic curve (at about 160 °C) can be attributed to the boundary between the two regions (Figure 2f). The KJMA model captures these two regimes. There is an important difference between nucleation in the coupling-limited 2D-NG and 1D-KJMA mechanisms. In the 2D-NG mechanism, nucleation involves the reversible formation of a transient state, which is attained by monomers diffusing in 2D, and a second irreversible step of coupling to form a dimer. In the KJMA model the term nucleus refers to a point in space at which the polymerization starts. Thus, the nucleation is the formation of the first C—C bond between two adjacent phenylenes, which in comparison to the NG mechanism occurs in a single step. These nuclei are distributed at random throughout the 1D chain.

Table 1. Extracted nucleation and growth (E_n, E_g) energies for dBB, dCB, BIB, and BCB using the coupling-limited NG model.

Molecule	Nucleation energy, E_n [eV]	Growth energy, E_g [eV]
dCB	1.33 ± 0.01	1.11 ± 0.01
dBB	1.29 ± 0.01	1.12 ± 0.01
BIB	1.15 ± 0.01	1.07 ± 0.01
BCB	1.25 ± 0.01	1.15 ± 0.01

The chemical reaction by a 1D-KJMA mechanism follows Equation (2)

$$X(T) = 1 - \exp\left[-N_0 l(T)\right] \quad (2)$$

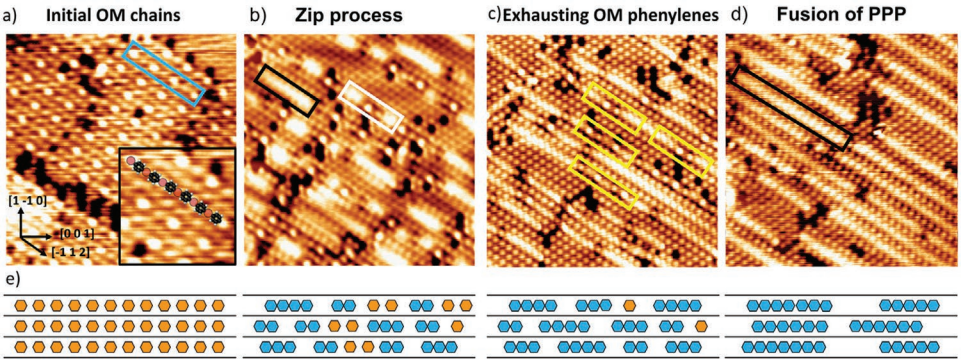

Figure 3. Thermal evolution of OM to PPP chains of dIB on Cu(110) monitored by STM. a) Initial assembly of OM chains after annealing to 100 °C (1 V, 0.2 nA) The inset, including a molecular model, shows the structure of the OM chain enclosed in the blue box. Transparent brown dots are Cu atoms between the consecutive phenylenes. b,c) Annealing at 200 °C leads to both the formation of short oligomers by coupling of adjacent monomers (b, 0.5 V, 1 nA) and oligomers growth until free monomers are exhausted (yellow boxes) (c, 0.01 V, 2 nA). d) Annealing to 250 °C yields the final PPP chains by fusion of oligomers (0.5 V, 0.2 nA). Blue and black boxes indicate organometallic chains and PPP chains, respectively. The white box shows oligomer fragments bonded together by Cu atoms. Yellow boxes show longer oligomer chains connected by Cu atoms. e) Schematic representation of the stages of OM to PPP chain conversion: orange and blue hexagons represent phenylene moieties in the OM and polymer phase, respectively. Black lines represent iodine rows. STM image size a–d): 6.3×6.3 nm^2.

where X is the fraction of polymer phase, N_0 is the density of initial nucleation sites and l is the chain length. The 1D-KJMA model describes the phenomena observed from the STM images (Figure 3) in which the coupling events can only occur within a single line of OM chains, and adjacent lines separated by iodine atoms mostly do not interact. Moreover, there is no dependence on the surface density of monomers, as is the case of the coupling-limited NG mechanism where the growth rate of the nucleus is linked to monomer diffusion by a random walk on the surface. The crucial difference between the precursors is that in the case of dIB the final PPP chains align along the same surface direction as the OM chains. The iodine atoms restrict monomers from leaving one OM chain to diffuse toward and join the monomers of neighboring chains. Thus, probability of finding an adjacent monomer within an OM chain is always equal to one (up to the completion of reaction). This implies that the fraction of polymer phase as a function of time changes as $dX/dt \propto NK(t)$, where N is the number of nucleation sites and $K(t)$ is the rate of attachment of monomers to the PPP nucleus. As the oligomer chain grows, the distance toward the next available monomer increases because the separation of the phenylenes in the polymer is smaller than that of the OM chain,[12a,21] so $K(t)$ is expected to decrease with increasing size of PPP nuclei. We assume $K(t) \propto dm/dt \propto 1/m(t)$, where m is the number of monomers in the PPP nucleus. In the framework of the 1D-KJMA model, we implemented this mechanistic picture using the following growth law in which the growth is limited as the length of the chain l increases

$$\frac{dl}{dT} = \frac{\nu}{l\phi(T)} e^{-Eg/RT} \tag{3}$$

where E_g is the activation energy for growth, ν is the pre-exponential factor, and ϕ(T) is the experimental heating rate. The derivation of the final equation for the fitting process and details of the fitting procedure can be found in Section 5 (Supporting Information) (Equation (S15), Supporting Information) and Section 3, respectively. Information on the experimental heating rate can be found in Section 2 (Supporting Information). The 1D-KJMA model fits the chemical reaction well, yielding a growth energy barrier of 0.95 ± 0.01 eV (Figure 2f) and an attempt frequency of 3.5×10^9 s^{-1} (Section 5 and Figure S6, Supporting Information). In contrast, this model is not able to reproduce the experimental kinetics of the other four precursors, which demonstrates the unique reaction mechanism of dIB (Figure S7, Supporting Information).

The key finding of the kinetic analysis of the TP-XPS maps is the differentiation of two distinct mechanistic regimes. On-surface Ullmann coupling is generally considered a diffusive process, in which dehalogenated molecules walk randomly on the surface until they find a partner for coupling.[9a,24] However, as our analysis of PPP formation from five different 1,4-dihalobenzenes demonstrates, this is not always the case. While four of the investigated precursors agree with coupling-limited NG kinetics, dIB polymerizes via a topotactic mechanism. The origin of this variance lies in the different arrangements of the OM and PPP chains for the five precursors. The initial OM chains obtained by using dBB, dCB, BIB, and BCB are aligned along the [1 –1 ±1] surface direction. On the contrary, OM chains obtained by using dIB run along the [1 –1 ±2] direction. The preferred orientation of the PPP chains is [1 –1 ±2] for all precursors as well as [1 –1 0] for BCB, dCB, and dIB.[21] In the case of dIB, however, we observe that the PPP chains primarily align along the [1 –1 0] direction at submonolayer coverages (Figure S8, Supporting Information), while they are already aligned along the PPP growth direction for one monolayer coverage, thus facilitating a topotactic reaction mechanism. Although iodine is present in the case of BIB, it does not exhibit topotactic growth or a mixture between topotactic growth and coupling-limited NG. The iodine tends to form isolated iodine islands and does not adsorb between the OM chains.[21] Thus, the self-assembly of OM chains involves bromine atoms and the system resembles dBB more than dIB and follows the NG mechanism.

TP-XPS and kinetic modeling established that there are two distinct kinetic mechanisms that drive the polymerization

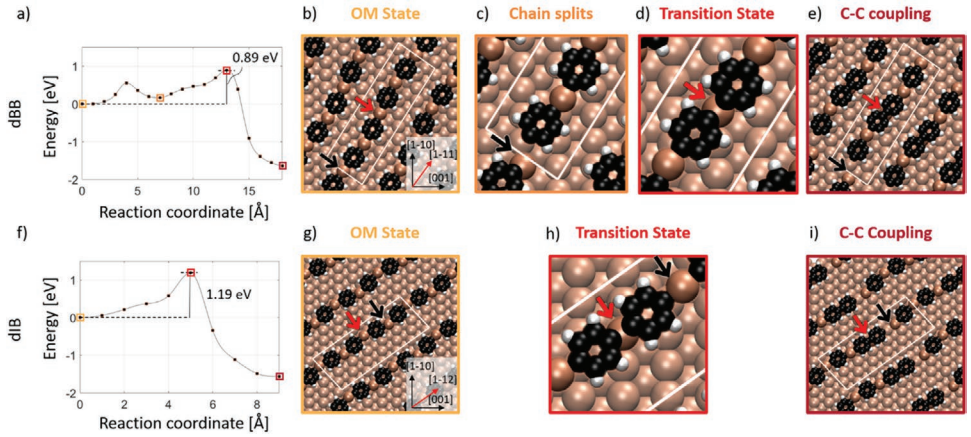

Figure 4. NEB modeling of the microscopic processes during dimerization along the [1 –1 ±1] (dBB) a–e) and [1 –1 ±2] (dIB) f–i) surface directions, in the absence of halogen atoms. Left graphs represent the minimum energy landscape for the coupling of two phenylenes, where the reaction coordinate is the total distance along the pathway(s) in the NEB calculations, and represents different atomic motions for each of the elementary steps in a). The colored boxes in a) and f) indicate significant geometries during the coupling process, shown to the right of the graphs. Brown spheres are Cu atoms, and a white parallelogram indicates the unit cell. For clarity, Cu atoms not bonded to phenylenes are shown with a lighter tone. Red and black arrows indicate the coupling site and the site at which the chain splits, respectively.

reaction. To identify the origin of this change, we studied the mechanistic picture of the dimerization of dBB (as an example of the precursors following the coupling-limited NG model) and dIB by investigating the effects of the different surface directions along which polymerization occurs and the effects of the halogens using NEB calculations. To differentiate between effects of the two surface alignments of the OM chains and the coadsorbed halogen atoms, we first analyzed coupling along the [1 –1 ±1] and [1 –1 ±2] surface direction in the absence of bromine or iodine atoms, respectively. The unit cell oriented along the [1 –1 ±1] surface direction corresponding to dBB consists of four phenylenes with a kink every fourth phenylene (**Figure 4**b).[12a] Three bridging Cu adatoms are located at short-bridge sites and the bridging Cu adatom at the kink is at a top site. For all calculations, OM Cu adatoms at short- or long-bridge sites are lifted surface atoms that return to their original surface position during polymerization. We considered coupling of a dimer in which the OM Cu is assumed to be an adatom, but found that ejection of the adatom during coupling involves an excessively high barrier of approximately 2.4 eV. The origin of the source of bridging metal atoms is still unsettled[25] and we thus followed the approach of lifting surface atoms.[12a,26]

We found that dimerization along [1 –1 ±1] occurs via two elementary steps (Figure 4a). The distance between two consecutive phenylenes is 2.2 Å larger in an OM chain than in a covalent dimer, so coupling requires the chain to break. The OM chain splitting occurs in the first step at the shared Cu atom which is at a top site, indicated by the black arrow in Figure 4b. This central phenylenes adjacent to the red arrow in Figure 4b are then able to approach and reach the transition state shown in Figure 4d, in which the shared Cu atom has returned to its initial surface site and the phenylenes are forming a covalent bond. Interestingly, the final dimer does not follow the original surface direction along [1 –1 ±1] but exhibits a rotation toward the [1 –1 ±2] surface direction (Figure 4e). The first elementary step of breaking the OM chain has an activation energy of 0.55 eV and is reversible due to its endothermic nature. The subsequent rate-determining step of C—C coupling has an activation energy of 0.73 eV, and the overall energy barrier for the dimerization process is 0.89 eV.

Next, we shed light on the mechanism of dimerization along the [1 –1 ±2] surface direction (corresponding to dIB), which was modeled by a unit cell consisting of four phenylenes (Figure 4g) with the organometallic Cu atoms located at alternating short-bridge and long-bridge sites. A cell smaller than the reported experimental unit cell containing seven phenylene molecules[21] was used to make the NEB calculations more tractable. The OM alignment along the [1 –1 ±2] surface direction is close in energy (0.014 eV per phenylene higher) to the OM alignment along [1 –1 ±1]. In stark contrast to the two-step pathway for the [1 –1 ±1] direction, dimerization along [1 –1 ±2] follows a single-step reaction with an energy barrier of 1.19 eV (Figure 4f). Here, the dimerization starts at the two central phenylenes indicated by the red arrow in Figure 4g. The phenylenes approach and the shared Cu atom at a short bridge site returns to its original surface location (Figure 4h). At the same time as the dimerization, the OM chain breaks at the top phenylene (black arrow Figure 4i) to compensate for the difference in distance between phenylenes in the OM chain and covalent dimer (Figure 4i). Whereas dimerization along [1 –1 ±1] requires rotation, coupling along [1 –1 ±2] occurs without a change in alignment of the phenylenes and thus is consistent with a topotactic mechanism.

The pathway analysis indicates that the direction of polymerization on Cu(110) determines the mechanism of dimerization. We then introduced halogen atoms to the respective systems to identify their influence on dimerization, again examining first the OM chain along [1 –1 ±1] that corresponds to dBB. We find that the inclusion of bromine atoms introduces an additional elementary step, as shown in the calculated coupling pathway (**Figure 5**a). Similar to the case without halogens, the OM chain first breaks at the shared Cu atom at the top site indicated by a black arrow in Figure 5b, which enables the later coupling of the center phenylenes (red arrow in Figure 5b). Figure 5c

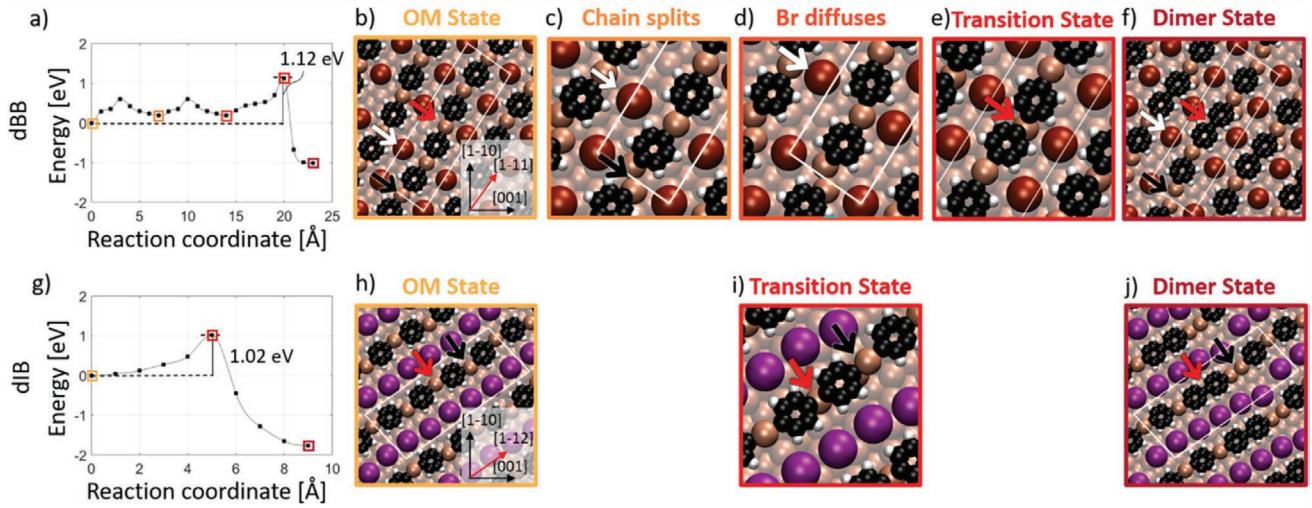

Figure 5. NEB modeling of the microscopic processes during dimerization along the [1 –1 ±1] (dBB) a–f) and [1 –1 ±2] (dIB) g–j) surface directions, including halogen atoms. Left graphs represent the minimum energy landscape for the coupling of two phenylenes, where the reaction coordinate is the total distance along the pathway(s) in the NEB calculations, and represents different atomic motions for each of the elementary steps. The colored boxes in a) and g) indicate significant geometries during the coupling process, shown to the right of the graphs. Red, purple, and brown spheres are bromine, iodine, and Cu atoms, respectively, and a white parallelogram indicates the unit cell. For clarity, Cu atoms not bonded to phenylenes are shown with a lighter tone. Red, black, and white arrows indicate the coupling site, the chain split site and the diffusing bromine atom, respectively.

shows this state in which the terminal phenylenes of the OM chain have ejected the shared surface atom and bond to two different surface atoms. In a second reversible elementary step a bromine atom shifts to the next short-bridge site along the row, which is marked by white arrows in Figure 5b–d. These elementary steps are difficult to measure by STM as they are likely to be short-lived and the OM chain is thermodynamically more stable, and reversibility is given due to the low activation energy for backwards diffusion. In the final, irreversible step, the center phenylenes couple and the dimer rotates toward the [1–1 ±2] surface direction.

Critically, the introduction of bromine atoms increases the activation energy to 1.12 eV and reduces the heat of reaction by 0.63 eV. We attribute these changes to steric repulsion between the OM chains and Br atoms in the transition state and final states. To identify the cause, we computed the interaction energies E_I between the OM chains and Br atoms for the initial and dimerized state, defined as the difference in energy between the coadsorbed OM chains and halogen atoms and the two adsorbed separately (see Computational Methods), and analyzed the charge densities and Br-phenylene distances. The interaction energy for the initial state is 0.99 eV per unit cell, reflecting a strong electrostatic attraction between the negatively charged (–0.5 e) chemisorbed Br atoms and the phenylenes (see Figure S9, Supporting Information).

This energy is much smaller in the dimerized state (0.34 eV per unit cell), and the bromine atoms and hydrogen atoms on the phenylene are significantly closer than the optimal Br···H distance (≈2.5 vs 3.0 Å; see Figures S10 and S11, Supporting Information). These Br···H distances are similar (2.6 Å) in the transition state, pointing to steric repulsion as the cause of the increased reaction barrier and the reduced heat of reaction. The dimerization also involves in-plane rotation of the reacting phenylenes by 14° from the initial alignment along the [1 –1 ±1] surface direction toward [1 –1 ±2]. As the polymerization progresses, the self-assembled phase along [1 –1 ±1] would become increasingly strained and thus polymerization along this surface direction would become unfavorable. The NEB calculations therefore rule out topotactic reaction for dBB, in contrast to dIB. We expect this effect to apply also to BIB, BCB, and dCB, which have a similar linear self-assembly following complete dehalogenation. Our modeling suggests that steric repulsion disfavors coupling from the initial self-assembly of dBB, so it is possible that the OM phase is disrupted before any dimerization occurs following the pathway simulated here. However, the attraction between Br atoms and phenylenes and their strong effect on the barrier indicates that the halogen atoms must be considered in modeling on-surface Ullmann reactions. We also examined coupling at the top site (the other possibility in the dBB unit cell) but identified a higher energy barrier (1.4 eV).

We completed the study by adding iodine atoms to the arrangement along the [1 –1 ±2] surface direction (Figure 5h). The polymerization occurs through very similar geometries as without halogens. Figure 5h shows the initial OM chains and the red and black arrow indicate the coupling and chain split sites, respectively. As the coupling phenylenes approach, the chain splits at the black arrow in Figure 5i to release the stress on the OM chain caused by the difference in bonding distance between the OM phenylenes and covalent dimer. After dimerization, the resulting chain made of OM phenylenes and a dimer follows the [1 –1 ±2] surface direction. Compared to the case without iodine, the energy barrier for dimerization is substantially lower at 1.02 eV (Figure 5g). The single-step pathway and activation energy for dimerization of dIB determined by NEB agrees with the results of the 1D-KJMA mechanistic model, and the theoretical identification of a catalytic effect of adjacent iodine atoms is consistent with the lower reaction temperature of iodine-containing precursors observed in the TP-XPS maps.

To obtain insights into the effect of iodine, we computed the interaction energies and charge density differences also for dIB. In the initial state, the interaction energy between iodine atoms and OM chains is 0.35 eV, which is significantly lower compared to the case of dBB, and reflects the smaller charge on the iodines (–0.3 e) and the larger I···H distances, which are greater than the optimal distance of 3.1 Å (see Figures S10 and S11, Supporting Information). In the transition state, the distances of adjacent I atoms to H atoms on the coupling phenylenes become closer to the equilibrium value, so we propose that the reduction in activation energy results from greater attraction between the iodine and phenylenes that stabilizes the transition state. Another possible explanation is a charge redistribution on the organometallic carbons that weakens the C-Cu bond (see Figure S9, Supporting Information). A similar redistribution is observed for dBB, however it could be a weaker effect than the steric repulsion that causes the barrier to increase. To rule out the possibility of coupling at the kink site for dIB that is present in the experimental unit cell, we created a supercell that includes this kink site with three phenylenes (Figure S12b, Supporting Information). Here, dimerization led to the displacement of the iodine atoms from their initial adsorption sites, which in a nonperiodic system would require an unfavorable disruption of the OM self-assembly (Figure S12a,b, Supporting Information). We therefore conclude that dimerization likely occurs along the pathway shown in Figure 5g, corresponding to coupling at short-bridge sites of the organometallic Cu adatoms.

To summarize, NEB calculations indicate that for OM chains without halogen atoms, coupling is favored along the [1 –1 ±1] surface direction over the [1 –1 ±2] direction. The addition of bromine atoms in the OM chains along [1 –1 ±1] destabilizes the transition state and increases the energy barrier for dimerization, whereas the addition of iodine atoms adjacent to OM chains along [1 –1 ±2] reduces the barrier to coupling. The calculated activation energies in the pathways including halogens are consistent with the experimental nucleation energies obtained from kinetic modeling. Finally, the geometries of the dimerization pathway of dBB do not favor topotactic growth, as suggested also by STM measurements, while the computed pathway of dIB supports a topotactic mechanism.

3. Conclusions and Perspectives

We discovered a topotactic Ullmann polymerization in a series of aryl halides and identified the cause of the change in kinetics by combining TP-XPS, STM, kinetic modeling and DFT calculations. Two reaction regimes are found, dominated by either topotactic conversion or diffusive coupling. In the case of dIB, we observed a topotactic reaction along a fixed surface direction guided by iodine confinement of the organic species, while the on-surface polymerization of dBB, dCB, BIB, and BCB follows the established coupling-limited NG kinetics mediated by transient states. NEB modeling indicates that coupling of dIB occurs between rows of iodine atoms in a single irreversible step with no change in the phenylene alignment, which is consistent with the 1D-KJMA model. Comparison with systems of isolated OM chains demonstrates that the coadsorbed halogen atoms have a strong influence on the reaction barrier, which is increased by bromine and decreased by iodine. The origin of this change in activation energy is linked to the repulsive/attractive forces between phenylene and halogens, which indicate a possible explanation for the choice of kinetic regime, in that the steric repulsion induced by dimerization of dBB prevents a topotactic reaction, whereas for dIB the phenylene-iodine interaction is unchanged by dimerization. Our work demonstrates the existence of topotactic reactions in surface-confined Ullmann coupling and emphasizes the important role of the halogen leaving group in on-surface reactions, effects that cannot be revealed by conventional STM alone, but instead require real-time insights into the polymerization mechanism. The control of self-assembly and reaction mechanism through the choice of halogen substituent could be applied to other precursors for surface-confined Ullmann coupling and other dehalogenative polymerizations. Halogen-controlled directionality of coupling therefore represents an original concept that could benefit the synthesis of extended surface-confined polymers.

4. Experimental Section

All experiments were carried out under ultrahigh vacuum (UHV) conditions with pressure below 2×10^{-10} mbar. The precursor molecules 1,4-dibromobenzene (98% purity), 1,4-dichlorobenzene (99%), 1,4-diiodobenzene (99%), 1-bromo-4-iodobenzene (98%), and 1-bromo-4-chlorobenzene (99%) were acquired from Sigma-Aldrich. Precursors were dosed by a leak valve on Cu(110) (from Surface Preparation Laboratory) held at room temperature (RT). The substrate was prepared by repeated Ar+ sputtering (1.2 keV) and annealing (500 °C). TP-XPS experiments were carried out at the ALOISA beamline of the Elettra synchrotron-radiation facility in Trieste (Italy), by means of a custom-made hemispherical electron analyzer equipped with a 2D delay-line detector (Sincrotrone Elettra S.C.p. A.). XPS measurements were performed with the analyzer oriented at normal emission, while keeping the sample at grazing incidence (4°). The C 1s core level was measured at $h\nu = 390$ eV in p-polarization. TP-XPS snapshot spectra with a kinetic energy bandwidth of ≈4 eV (overall energy resolution of 350 meV) were recorded each second, while progressively increasing the temperature by radiative heating (filament) from RT to 250 °C. TP-XPS measurements were carried out with a constant current to the filament, which reaches a maximum temperature of 250 °C. Reference calibration spectra have been also measured with an overall resolution of 200 meV. The temperature was measured by a K type thermocouple (Chromel-Alumel) in direct contact with the sample. STM experiments were carried out using an Omicron LT-STM at a temperature of 5 K. Bias voltages are applied to the sample.

Computational Methods: Theoretical calculations were performed using the Vienna Ab-initio Simulation Package (VASP)[27] using the Perdew–Burke–Ernzerhof[28] generalized-gradient approximation (PBE-GGA) for the exchange-correlation potential, the projector augmented wave (PAW) method,[29] and a plane-wave cutoff of 450 eV. The zero-damping DFT-D3 method of Grimme[30] was used for the van der Waals (vdW) correction of the potential energy. The dimerization pathways for dIB were computed using the climbing-image NEB method.[31] Cu(110) slabs were constructed using a lattice constant of 0.363 nm and a 1.8 nm vacuum layer, corresponding to a (2, 2 | –4, 9) epitaxy matrix for dBB and a (1, 4 | –6, 6) matrix for dIB, with five atomic layers and the positions of the bottom two atomic layers fixed. The NEB calculation for coupling of OM chains aligned along [1 –1 ±1] was divided into two pathways with eight intermediate images each for the OM chain splitting and coupling, respectively. The calculation for the dimerization including Br atoms for dBB was divided into three pathways with 6, 6, and 8 intermediate images

for the OM chain splitting, Br diffusion, and coupling respectively. For dIB, eight intermediate images were used for both pathways, without or with I atoms. Possible reaction pathways were evaluated using the gamma k-point and the final pathways optimized using a $3 \times 6 \times 1$ k-point mesh until the force on each atom was below 0.02 eV Å^{-1}. The interaction energy E_I was computed by comparing the energies of optimized geometries for OM chains and halogens in the same or different supercells, corresponding to $E_I = E_{OM+X,\,ad} + E_{Cu\,slab} - (E_{OM,ad} + E_{X,ad})$, and the difference in energy between OM chains aligned along [1 −1 ±2] and [1 −1 ±1] was determined by comparing the adsorption energies of OM chains in each supercell. The charge density analysis for the effect of the halogen atoms compared the combined OM and halogen self-assembly to isolated adsorbed OM chains and halogen atoms in vacuum, i.e., $\Delta\rho = \rho_{OM+X,\,ad} - \rho_{OM,ad} - \rho_{X,vac}$. The interaction energies and OM chain adsorption energies were computed using a $5 \times 10 \times 1$ k-point mesh and the charge densities using the gamma k-point. Morse potential calculations to estimate the equilibrium X···H distances were calculated by optimizing the geometry of a gas-phase phenylene and X-Cu molecule (to represent a chemisorbed X atom) and then freezing the coordinates and scanning the X···H distance, with gamma k-point sampling. Images of the calculated structures were generated using the VMD software.[32]

Supporting Information

Supporting Information is available from the Wiley Online Library or from the author.

Acknowledgements

This work was partially supported by the project Grande Rilevanza Italy-Quebec of the Italian Ministero degli Affari Esteri e della Cooperazione Internazionale (MAECI), Direzione Generale per la Promozione del Sistema Paese. The authors acknowledge beamtime access and support from the Elettra light source in Italy. F.R. is grateful to the Canada Research Chairs program for partial salary support. D.F.P. and F.R. acknowledge funding from NSERC (individual Discovery Grants) and from an FRQNT team grant.

Conflict of Interest

The authors declare no conflict of interest.

Data Availability Statement

Research data are not shared.

Keywords

density functional calculations, kinetics, reaction mechanisms, surface chemistry, time-resolved spectroscopy

Received: May 25, 2021
Revised: July 21, 2021

[1] G. Galeotti, F. De Marchi, E. Hamzehpoor, O. MacLean, M. Rajeswara Rao, Y. Chen, L. V. Besteiro, D. Dettmann, L. Ferrari, F. Frezza, P. M. Sheverdyaeva, R. Liu, A. K. Kundu, P. Moras, M. Ebrahimi, M. C. Gallagher, F. Rosei, D. F. Perepichka, G. Contini, *Nat. Mater.* **2020**, *19*, 874.

[2] S. Mishra, D. Beyer, K. Eimre, S. Kezilebieke, R. Berger, O. Gröning, C. A. Pignedoli, K. Müllen, P. Liljeroth, P. Ruffieux, X. Feng, R. Fasel, *Nat. Nanotechnol.* **2020**, *15*, 22.

[3] a) O. Gröning, S. Wang, X. Yao, C. A. Pignedoli, G. Borin Barin, C. Daniels, A. Cupo, V. Meunier, X. Feng, A. Narita, K. Müllen, P. Ruffieux, R. Fasel, *Nature* **2018**, *560*, 209; b) D. J. Rizzo, G. Veber, T. Cao, C. Bronner, T. Chen, F. Zhao, H. Rodriguez, S. G. Louie, M. F. Crommie, F. R. Fischer, *Nature* **2018**, *560*, 204; c) Z. A. Gao, C.-H. Hsu, J. Liu, F.-C. Chuang, R. Zhang, B. Xia, H. Xu, L. Huang, Q. Jin, P. N. Liu, N. Lin, *Nanoscale* **2019**, *11*, 878; d) B. Cirera, A. Sánchez-Grande, B. de la Torre, J. Santos, S. Edalatmanesh, E. Rodríguez-Sánchez, K. Lauwaet, B. Mallada, R. Zbořil, R. Miranda, O. Gröning, P. Jelínek, N. Martín, D. Ecija, *Nat. Nanotechnol.* **2020**, *15*, 437.

[4] Y. Zhong, B. Cheng, C. Park, A. Ray, S. Brown, F. Mujid, J.-U. Lee, H. Zhou, J. Suh, K.-H. Lee, A. J. Mannix, K. Kang, S. J. Sibener, D. A. Muller, J. Park, *Science* **2019**, *366*, 1379.

[5] T. Wang, J. Huang, H. Lv, Q. Fan, L. Feng, Z. Tao, H. Ju, X. Wu, S. L. Tait, J. Zhu, *J. Am. Chem. Soc.* **2018**, *140*, 13421.

[6] a) J. Björk, Y.-Q. Zhang, F. Klappenberger, J. V. Barth, S. Stafström, *J. Phys. Chem. C* **2014**, *118*, 3181; b) T. Lin, L. Zhang, J. Björk, Z. Chen, M. Ruben, J. V. Barth, F. Klappenberger, *Chem. – Eur. J.* **2017**, *23*, 15588.

[7] M. Yu, C. Chen, Q. Liu, C. Mattioli, H. Sang, G. Shi, W. Huang, K. Shen, Z. Li, P. Ding, P. Guan, S. Wang, Y. Sun, J. Hu, A. Gourdon, L. Kantorovich, F. Besenbacher, M. Chen, F. Song, F. Rosei, *Nat. Chem.* **2020**, *12*, 1035.

[8] a) M. Lackinger, *Chem. Commun.* **2017**, *53*, 7872; b) M. Di Giovannantonio, G. Contini, *J. Phys.: Condens. Matter* **2018**, *30*, 093001.

[9] a) M. Bieri, M.-T. Nguyen, O. Gröning, J. Cai, M. Treier, K. Aït-Mansour, P. Ruffieux, C. A. Pignedoli, D. Passerone, M. Kastler, K. Müllen, R. Fasel, *J. Am. Chem. Soc.* **2010**, *132*, 16669; b) J. Eichhorn, D. Nieckarz, O. Ochs, D. Samanta, M. Schmittel, P. J. Szabelski, M. Lackinger, *ACS Nano* **2014**, *8*, 7880; c) M. O. Blunt, J. C. Russell, N. R. Champness, P. H. Beton, *Chem. Commun.* **2010**, *46*, 7157; d) L. Lafferentz, V. Eberhardt, C. Dri, C. Africh, G. Comelli, F. Esch, S. Hecht, L. Grill, *Nat. Chem.* **2012**, *4*, 215; e) L. Grill, M. Dyer, L. Lafferentz, M. Persson, M. V. Peters, S. Hecht, *Nat. Nanotechnol.* **2007**, *2*, 687; f) J. A. Lipton-Duffin, O. Ivasenko, D. F. Perepichka, F. Rosei, *Small* **2009**, *5*, 592; g) T. A. Pham, B. V. Tran, M.-T. Nguyen, M. Stöhr, *Small* **2017**, *13*, 1603675.

[10] a) X.-Y. Wang, J. I. Urgel, G. B. Barin, K. Eimre, M. Di Giovannantonio, A. Milani, M. Tommasini, C. A. Pignedoli, P. Ruffieux, X. Feng, R. Fasel, K. Müllen, A. Narita, *J. Am. Chem. Soc.* **2018**, *140*, 9104; b) J. Cai, P. Ruffieux, R. Jaafar, M. Bieri, T. Braun, S. Blankenburg, M. Muoth, A. P. Seitsonen, M. Saleh, X. Feng, K. Müllen, R. Fasel, *Nature* **2010**, *466*, 470; c) Z. Chen, H. I. Wang, N. Bilbao, J. Teyssandier, T. Prechtl, N. Cavani, A. Tries, R. Biagi, V. De Renzi, X. Feng, M. Kläui, S. De Feyter, M. Bonn, A. Narita, K. Müllen, *J. Am. Chem. Soc.* **2017**, *139*, 9483; d) Z. Chen, H. I. Wang, J. Teyssandier, K. S. Mali, T. Dumslaff, I. Ivanov, W. Zhang, P. Ruffieux, R. Fasel, H. J. Räder, D. Turchinovich, S. De Feyter, X. Feng, M. Kläui, A. Narita, M. Bonn, K. Müllen, *J. Am. Chem. Soc.* **2017**, *139*, 3635.

[11] C. Moreno, M. Vilas-Varela, B. Kretz, A. Garcia-Lekue, M. V. Costache, M. Paradinas, M. Panighel, G. Ceballos, S. O. Valenzuela, D. Peña, A. Mugarza, *Science* **2018**, *360*, 199.

[12] a) M. Di Giovannantonio, M. El Garah, J. Lipton-Duffin, V. Meunier, L. Cardenas, Y. Fagot Revurat, A. Cossaro, A. Verdini, D. F. Perepichka, F. Rosei, G. Contini, *ACS Nano* **2013**, *7*, 8190; b) M. Di Giovannantonio, M. El Garah, J. Lipton-Duffin, V. Meunier, L. Cardenas, Y. Fagot-Revurat, A. Cossaro, A. Verdini, D. F. Perepichka, F. Rosei, G. Contini, *ACS Nano* **2014**, *8*, 1969;

c) W. Wang, X. Shi, S. Wang, M. A. Van Hove, N. Lin, *J. Am. Chem. Soc.* **2011**, *133*, 13264; d) M. Chen, J. Xiao, H.-P. Steinrück, S. Wang, W. Wang, N. Lin, W. Hieringer, J. M. Gottfried, *J. Phys. Chem. C* **2014**, *118*, 6820.

[13] a) C. Anichini, W. Czepa, D. Pakulski, A. Aliprandi, A. Ciesielski, P. Samorì, *Chem. Soc. Rev.* **2018**, *47*, 4860; b) M. Gobbi, E. Orgiu, P. Samorì, *Adv. Mater.* **2018**, *30*, 1706103; c) K. Müller, M. Enache, M. Stöhr, *J. Phys.: Condens. Matter* **2016**, *28*, 153003; d) G. Shi, J. Zhou, Z. Li, Y. Sun, L. N. Kantorovich, Q. Fang, F. Besenbacher, M. Yu, *Angew. Chem., Int. Ed.* **2020**, *59*, 15958.

[14] a) G. Galeotti, F. De Marchi, T. Taerum, L. V. Besteiro, M. El Garah, J. Lipton-Duffin, M. Ebrahimi, D. F. Perepichka, F. Rosei, *Chem. Sci.* **2019**, *10*, 5167; b) C. Steiner, J. Gebhardt, M. Ammon, Z. Yang, A. Heidenreich, N. Hammer, A. Görling, M. Kivala, S. Maier, *Nat. Commun.* **2017**, *8*, 14765.

[15] Y.-L. Zhu, H.-Y. Zhao, C.-L. Fu, Z.-W. Li, Z.-Y. Sun, *Nanoscale* **2020**, *12*, 22107.

[16] R. D. Shannon, R. C. Rossi, *Nature* **1964**, *202*, 1000.

[17] a) P. C. M. Grim, S. De Feyter, A. Gesquière, P. Vanoppen, M. Rüker, S. Valiyaveettil, G. Moessner, K. Müllen, F. C. De Schryver, *Angew. Chem., Int. Ed. Engl.* **1997**, *36*, 2601; b) Y. Yang, M. B. Zimmt, *Langmuir* **2015**, *31*, 12408.

[18] F. Sedona, M. M. S. Fakhrabadi, S. Carlotto, E. Mohebbi, F. De Boni, S. Casalini, M. Casarin, M. Sambi, *Phys. Chem. Chem. Phys.* **2020**, *22*, 12180.

[19] J. Sakamoto, J. van Heijst, O. Lukin, A. D. Schlüter, *Angew. Chem., Int. Ed.* **2009**, *48*, 1030.

[20] M. Di Giovannantonio, M. Tomellini, J. Lipton-Duffin, G. Galeotti, M. Ebrahimi, A. Cossaro, A. Verdini, N. Kharche, V. Meunier, G. Vasseur, Y. Fagot-Revurat, D. F. Perepichka, F. Rosei, G. Contini, *J. Am. Chem. Soc.* **2016**, *138*, 16696.

[21] G. Galeotti, M. Di Giovannantonio, J. Lipton-Duffin, M. Ebrahimi, S. Tebi, A. Verdini, L. Floreano, Y. Fagot-Revurat, D. F. Perepichka, F. Rosei, G. Contini, *Faraday Discuss.* **2017**, *204*, 453.

[22] G. Galeotti, M. Di Giovannantonio, A. Cupo, S. Xing, J. Lipton-Duffin, M. Ebrahimi, G. Vasseur, B. Kierren, Y. Fagot-Revurat, D. Tristant, V. Meunier, D. F. Perepichka, F. Rosei, G. Contini, *Nanoscale* **2019**, *11*, 7682.

[23] M. Fanfoni, M. Tomellini, *Il Nuovo Cimento D* **1998**, *20*, 1171.

[24] a) S. Clair, D. G. de Oteyza, *Chem. Rev.* **2019**, *119*, 4717; b) A. Rastgoo Lahrood, J. Björk, W. M. Heckl, M. Lackinger, *Chem. Commun.* **2015**, *51*, 13301.

[25] C. J. Judd, F. L. Q. Junqueira, S. L. Haddow, N. R. Champness, D. A. Duncan, R. G. Jones, A. Saywell, *Commun. Chem.* **2020**, *3*, 166.

[26] D. Barton, H.-Y. Gao, P. A. Held, A. Studer, H. Fuchs, N. L. Doltsinis, J. Neugebauer, *Chem. – Eur. J.* **2017**, *23*, 6190.

[27] a) G. Kresse, J. Hafner, *Phys. Rev. B* **1993**, *47*, 558; b) G. Kresse, J. Furthmüller, *Phys. Rev. B* **1996**, *54*, 11169.

[28] J. P. Perdew, M. Ernzerhof, K. Burke, *J. Chem. Phys.* **1996**, *105*, 9982.

[29] a) P. E. Blöchl, *Phys. Rev. B* **1994**, *50*, 17953; b) G. Kresse, D. Joubert, *Phys. Rev. B* **1999**, *59*, 1758.

[30] S. Grimme, J. Antony, S. Ehrlich, H. Krieg, *J. Chem. Phys.* **2010**, *132*, 154104.

[31] G. Henkelman, B. P. Uberuaga, H. Jónsson, *J. Chem. Phys.* **2000**, *113*, 9901.

[32] W. Humphrey, A. Dalke, K. Schulten, *J. Mol. Graph.* **1996**, *14*, 33.